Ingeniería y Universidad
ENGINEERING FOR DEVELOPMENT

Vol. 29
Continuous Publication
2025

ISSN: 2011-2769 (Online) | ISSN: 0123-2126 (Print)

Artículos

Numerical Simulation of Adobe Wallettes under Compression and Diagonal Tension with and without Reinforcement of Spaced *Guadua angustifolia* Kunth Strips*

Simulación numérica de muretes de adobe a compresión y tensión diagonal con y sin refuerzo de tiras espaciadas de *Guadua angustifolia* Kunth

DOI: https://doi.org/10.11144/Javeriana.iued29.nsaw

Jonathan Danilo Perilla Novoa [a]
Universidad Nacional de Colombia, Colombia
jperilla@unal.edu.co
ORCID: https://orcid.org/0009-0001-2872-9608

Juan Esteban Muñoz Rodríguez
Universidad Nacional de Colombia, Colombia
ORCID: https://orcid.org/0009-0008-2700-5238

Maritzabel Molina Herrera
Universidad Nacional de Colombia, Colombia
ORCID: https://orcid.org/0000-0003-2457-2815

Caori Patricia Takeuchi Tam
Universidad Nacional de Colombia, Colombia
ORCID: https://orcid.org/0000-0002-6273-7118

Received: 23 november 2024
Accepted: 29 august 2025
Published: 29 september 2025

Abstract:

Objective: This research aims to evaluate the effect of *Guadua angustifolia* Kunth strip reinforcement on the mechanical behavior of adobe wallettes subjected to compression and diagonal tension. *Materials and Methods*: Experimental tests on unreinforced and reinforced adobe wallettes were complemented with numerical simulations using the finite element method (FEM) and the microplane damage model, chosen for its ability to capture nonlinear tensile and compressive responses in quasi-brittle materials. *Results and Discussion*: The analyses showed that all reinforcement configurations improved the mechanical performance of adobe wallettes compared to unreinforced ones, with differences depending on strip inclination. *Conclusion*: Among the evaluated configurations, the vertical 90° arrangement proved the most effective, combining improved strength and stiffness with greater constructability.
Keywords: Adobe, Guadua Strips, Failure Mechanism, Finite Element Method (FEM).

Resumen:

Objetivo: Esta investigación tiene como propósito evaluar el efecto del refuerzo con tiras de *Guadua angustifolia* Kunth en el comportamiento mecánico de muretes de adobe sometidos a compresión y tensión diagonal. *Materiales y métodos*: Se realizaron ensayos experimentales en muretes de adobe sin refuerzo y con refuerzo, complementados con simulaciones numéricas mediante el método de elementos finitos (MEF) y el modelo de daño de microplano, seleccionado por su capacidad de representar respuestas no lineales a tracción y compresión en materiales cuasifrágiles. *Resultados y discusión*: Los análisis mostraron que todas las configuraciones de refuerzo mejoraron el desempeño mecánico de los muretes respecto a los no reforzados, con variaciones según la inclinación de las tiras. *Conclusión*: Entre las configuraciones evaluadas, la disposición vertical a 90° resultó la más efectiva, al combinar mayor resistencia y rigidez con facilidad constructiva.
Palabras clave: Adobe, Tiras de Guadua, Mecanismo de Falla, Método de Elementos Finitos (FEM).

Introduction

Adobe is a material composed of compressed soil, water, and either natural or artificial fibers [1]. It has been employed since prehistoric times in the construction of enduring structures, some of which still stand

Author notes

[a]Corresponding author. E-mail: jperilla@unal.edu.co

currently [2]. Its abundance and low cost make it a viable material for housing construction, particularly in rural areas where adobe buildings offer significant environmental benefits [3], [4]. However, adobe buildings have low mechanical resistance to seismic events and, because of that, require reinforcement through various techniques [5], [6], [7]. *Guadua angustifolia* Kunth (*Guadua*), known for its low density, moisture absorption, and high tensile strength, is a lightweight, accessible, and cost-effective material that shows strong potential as reinforcement in construction, aligning with the growing interest in renewable resources for sustainable development [8].

Research on adobe primarily involves its mechanical characterization, conducted through a range of experimental tests that measure attributes such as the elastic modulus, compressive strength, and maximum tension [9], [10], [11]. However, since adobe is essentially composed of soil, its properties heavily depend on the soil characteristics at the extraction site, leading to a broad range of values, which complicates precise comparisons between different types of adobe [12]. Regarding reinforcement, studies have analyzed the use of fibers from synthetic or natural materials to enhance their mechanical performance since the material's initial elaboration phase [13], [14], [15], [16]. Nonetheless, there is sparse research about retrofitting earth-built houses [17], [18], [19]. using sustainable materials such as *Guadua*, despite its widespread use in Colombian earth structures [20].

Experimental data and numerical simulations allowed understanding the interaction between adobe and *Guadua* strips as potential reinforcement for retrofitting such structures [21]. The research included finite element analysis to characterize adobe as a constituent material and to evaluate the mechanical behavior of adobe blocks subjected to compression and diagonal tension [22], [23]. Drawing on the microplane model [24], the study explored failure mechanisms and evaluated various angular configurations of *Guadua* strips to determine their optimal arrangement as structural reinforcement in adobe constructions.

Methodology

This section describes the methodology used to perform numerical simulations, grounded in experimental laboratory results to ensure a realistic representation of adobe structures. The process began with the simulation of an adobe unit (adobe block) 350 mm in length, 170 mm wide, and 100 mm in thickness, which serves as the basic component of the wallettes. Accurate modeling of contacts and boundary conditions was prioritized, including the implementation of steel plates to replicate laboratory constraints.

Based on the results of a sensitivity analysis, a mesh element size of 15 mm was adopted for all simulations. The initial calibration established the linear elastic properties, including Young's modulus (E) and Poisson's ratio (ν). For the nonlinear range, the constitutive model described in the following section was employed, accurately replicating the mechanical behavior observed in experimental tests.

Plasticity-damage microplane model

Finite element methods are valuable tools for characterizing and analyzing the mechanical behavior of various materials. Within a broad spectrum of finite element strategies, nonlinear analysis plays a pivotal role, particularly in implementing damage and plasticity models. These methodologies provide a deeper understanding of material failure under different loading conditions and cycles. Numerous elastoplastic damage models have been developed [25], [26], [27], [28], [29], [30]. and the implementation in finite element programs has been widely studied [31], [32], [33].

To carry out the failure analysis on the adobe unit and wallettes, the microplane plasticity–damage model reported in [24]. was employed. This model defines stress–strain relations on multiple oriented planes—known as microplanes—allowing the simulation of directional cracking, frictional slip, and compression

splitting, which are characteristic of quasi-brittle materials like adobe [23], [24]. The model was selected over other plastic-damage formulations due to its ability to independently represent tensile and compressive responses and to handle complex nonlinear behavior under cyclic or combined loading conditions [34].

Additionally, the model includes a separation of damage mechanisms in tension and compression, allowing for more accurate stress redistribution during cracking. It also incorporates implicit gradient enrichment to mitigate numerical instability and mesh sensitivity. Implemented in the ANSYS 2022 R1 finite element software, this model has been validated in applications involving heterogeneous granular materials like concrete and is applied here to adobe.

To analyze the adobe units with the microplane plasticity–damage model, the parameters presented in Table 1 were defined, including Young's modulus (E) and Poisson's ratio (ν), which were directly calculated from laboratory results. Other parameters, such as compressive strength (f_c, f_b), tension strength (f_t), and non-local parameters (R_t, D, σ_{cv}, R_c, γ_t, γ_c, β_t, β_c), were derived through model calibration based on experimental data.

TABLE 1
General parameters of the microplane model used for both adobe units and mortar

Parameter	Description
E	Young's modulus [MPa]
ν	Poisson's ratio [-]
f_c	Uniaxial compressive strength [MPa]
f_b	Biaxial compressive strength [MPa]
f_t	Tensile strength [MPa]
R_t	Tension cap hardening constant [-]
D	Compressive hardening constant [MPa^2]
σ_{cv}	Intersection between compression and yield limits [MPa]
R_c	Compression cap ratio constant [-]
γ_t	Tensile damage threshold [-]
γ_c	Compressive damage threshold [-]
β_t	Tension damage evolution [-]
β_c	Compression damage evolution [-]

Source: Authors own creation.

The experimental results were obtained from three laboratory tests conducted on real adobe blocks, collectively referred to as the Block Compression Test (BCT). Each test, labeled as BCT1, BCT2, and BCT3, produced load versus displacement curves. Since the tests involve compression, the material experiences a reduction in length along the loading axis, resulting in a negative displacement commonly referred to as shortening. Accordingly, Figure 1, along with subsequent figures for other tests, presents load versus shortening graphs. From these experimental results, an average curve (BCT) was derived to represent the overall behavior of the material under compression. This curve was then used to calibrate the model, resulting in the numerical curve labeled BCS (Block Compression Simulation), which accurately replicates the mechanical behavior observed during the laboratory tests.

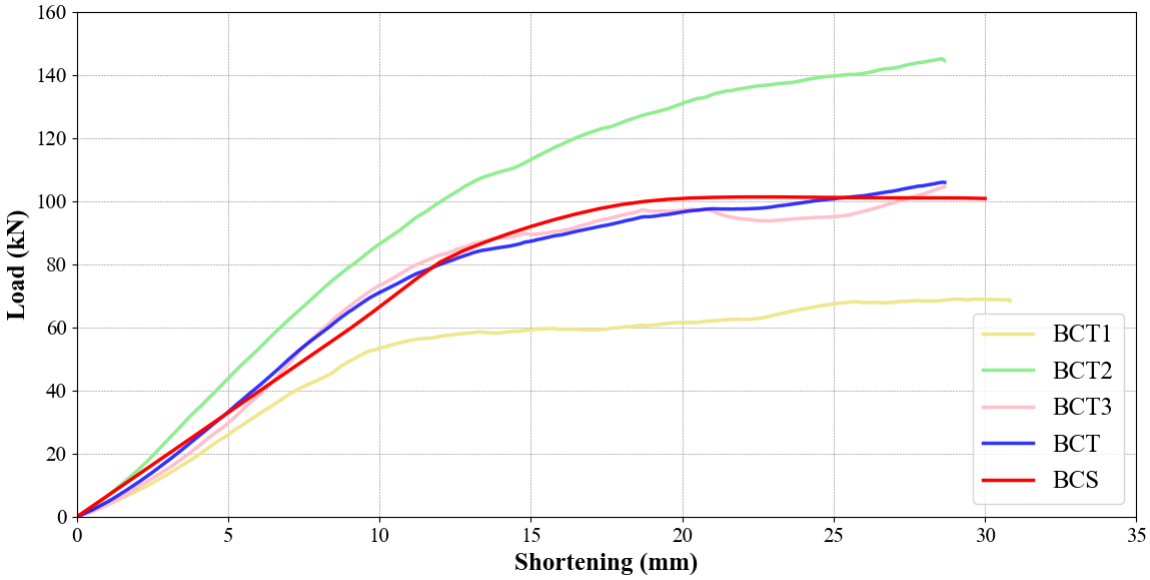

FIGURE 1
Compression adobe block model
Source: Authors own creation.

Following the calibration of the adobe block model, the adobe wallette model was developed. It consists of five rows of one-and-a-half blocks, joined by a soil-based paste; hereafter referred to as mortar. This mortar is a non-cementitious mixture of clay, sand, and natural fibers, applied to the contact surfaces of the blocks. The soil used in the paste is classified as A-6 clayey soil with a group index of 0 (AASHTO classification) and as CL, indicating low-compressibility clay, in the Unified Soil Classification System (USCS), with an initial absorption rate of 0.0024 g/cm^2/min [21]. As an alternative to cement, this paste bonds the blocks and enhances structural resistance, as will be discussed further.

Using a similar methodology to the block model, meshing, contact conditions, and other critical aspects were carefully defined to ensure the accurate performance of the wallette model. Simulations of compression and diagonal tension tests were conducted, utilizing calibration derived from experimental data. As with the adobe block simulation, linear and nonlinear parameters, as shown in Table 1, were set to calibrate the tests. The compressive strength parameters (f_c, f_b) were established through numerical calibration of the experimental compression wallette tests, while the tension strength parameter (ft) was determined from the results of diagonal tension. Lastly, the non-local parameters, such as (R_t, D, σ_{cv}, R_c, γ_t, γ_c, β_t, β_c), can't be regarded as singular to the material as they fluctuate depending on the type of test conducted on the materials. The overall procedure for defining and calibrating material properties is summarized in Figure 2.

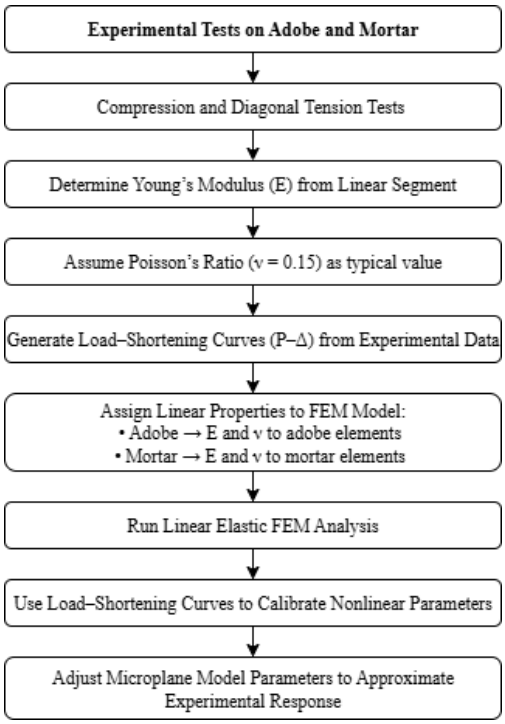

FIGURE 2

Flowchart of the procedure for assigning material properties and calibrating the numerical model

Source: Authors own creation.

Compression test simulation

Based on the load-displacement graphs obtained in the compression test of five unreinforced wallettes (UWCT), polynomial functions of the mechanical behavior of each one were defined to generate an average curve used for calibrating the numerical model. From these experimental tests, the behavior within the linear range was ascertained via numerical simulation, resulting in the derivation of elasticity and Poisson's ratio. Afterwards, the microplane model was employed to define the wallette's behavior within the nonlinear range. Following the calibration of the model pertaining to the non-reinforced wallette under compression, a similar procedure was applied with the experimental data of three tests on wallettes with vertically oriented *Guadua* strips reinforcement. The mean curve was defined, and the model shown in Figure 3 was developed.

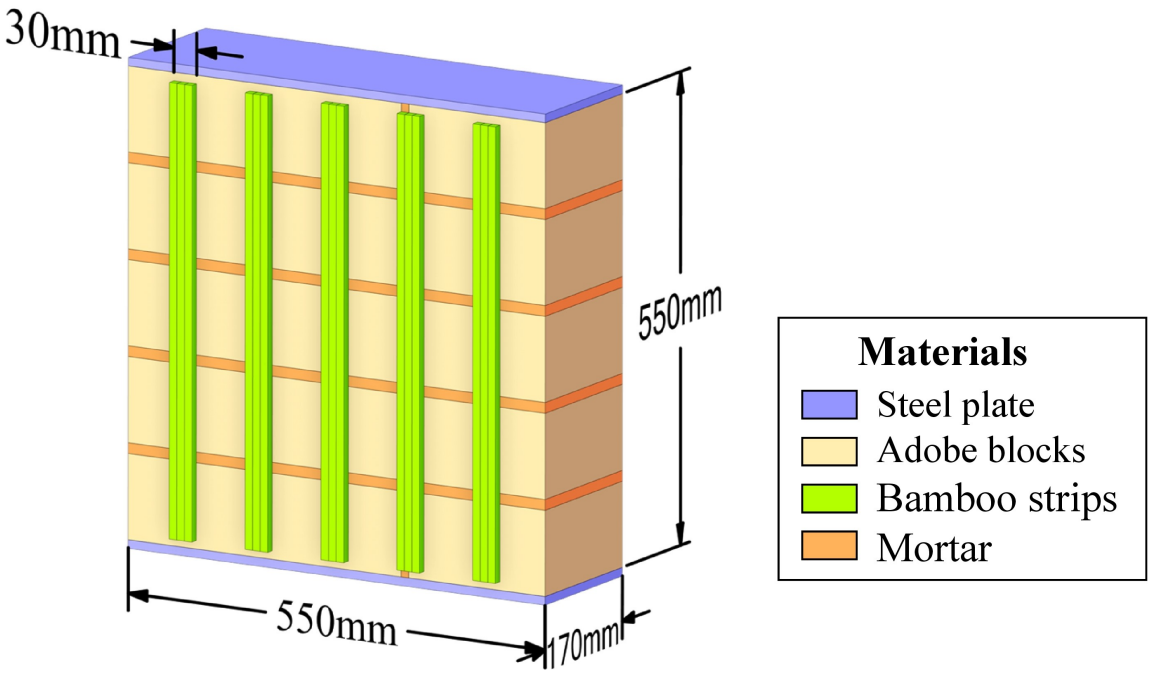

FIGURE 3
Reinforced adobe wallette model for compression testing
Source: Authors own creation.

In the elastic range, the modulus of elasticity and Poisson's ratio were determined for adobe blocks, mortar, and *Guadua* strips. After calibrating the model of the compression wallette reinforced with vertical *Guadua* strips, variations were made in the orientation of these strips, changing their inclination concerning the horizontal plane to establish the influence of the inclination of the strip on the mechanical behavior of the wallette; the different inclinations are shown in Figure 4.

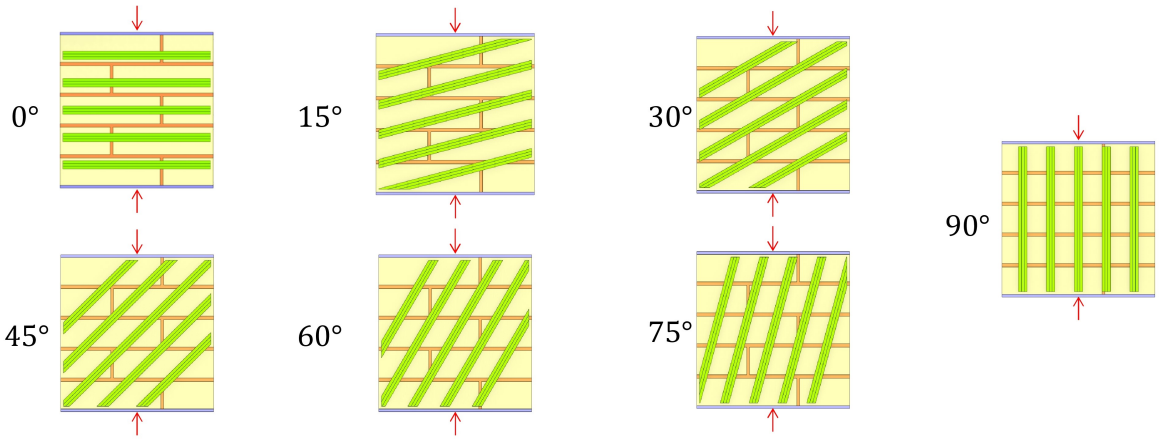

FIGURE 4
Models4of reinforced wallettes with different inclinations of Guadua strips for compression testing
Source: Authors own creation.

Diagonal tension test simulation

The diagonal tension test serves to determine the masonry shear strength and stiffness, subjecting these specimens to a compressive load along their diagonals as shown in Figure 5. This load generates tension

stresses perpendicular to the direction of the load. The type of failure that occurs in the specimen varies according to the composition of the materials.

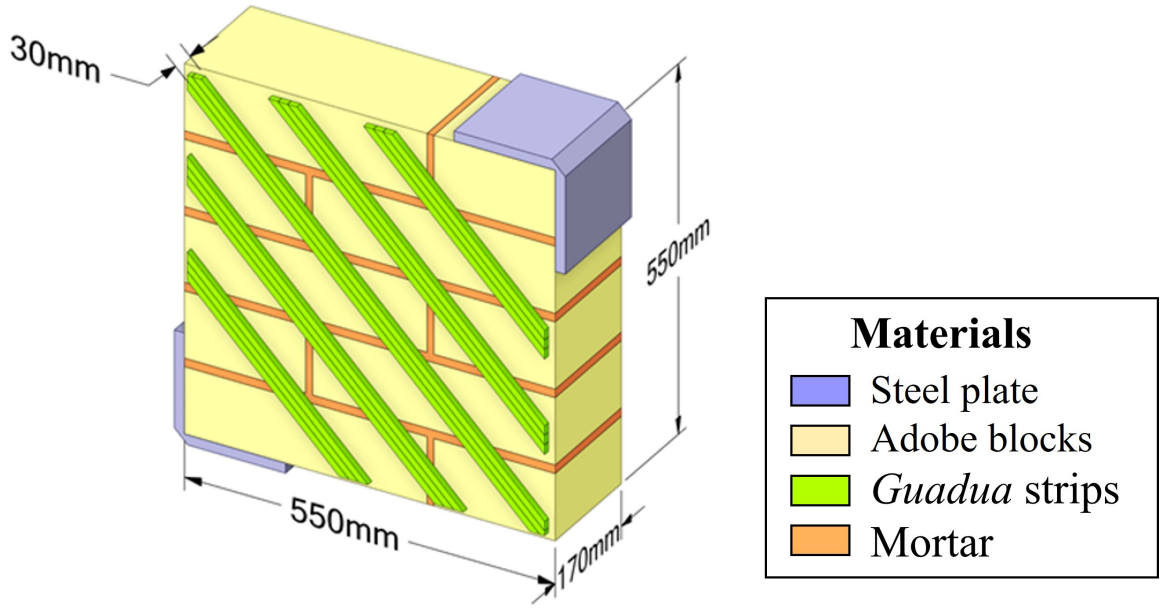

FIGURE 5
Reinforced adobe wallette model for diagonal tension testing
Source: Authors own creation.

Experimentally, the results of three tests of wallettes without reinforcement were compiled. From these, load and displacement (shortening) curves were extracted. These were approximated through polynomial functions and averaged to obtain a reference curve (UWDTT, Unreinforced wallette diagonal tension test), as can be shown in Figure 6.

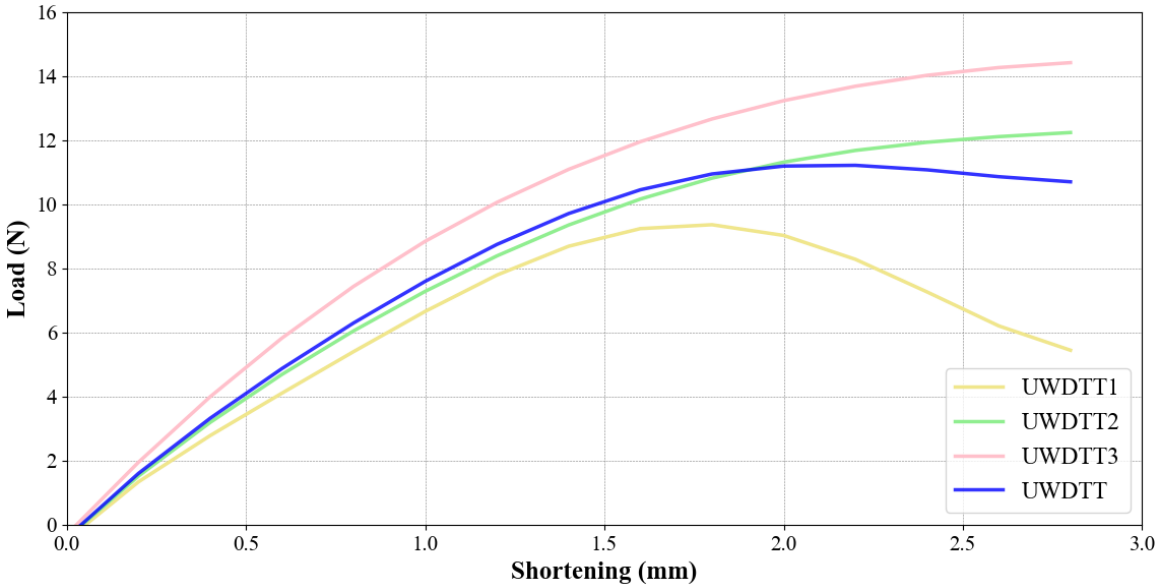

FIGURE 6
Unreinforced wallette diagonal tension
Source: Authors own creation.

As with the compression wallette, the analysis was initially conducted within the linear elastic range. To define the elastic behavior of the wall model, the modulus of elasticity (E) and Poisson's ratio (ν) were first determined individually for both the adobe units and the mortar. These values were obtained from the initial (linear) portion of the stress–strain curves derived from compression tests performed on each component separately. Once calibrated, the values were assigned to their corresponding domains in the finite element wallette model to ensure an accurate representation of each material's contribution to the global response.

Subsequently, the microplane model was applied to define the behavior of the wallette in the nonlinear range. After having calibrated the model of the unreinforced wallette, simulations were carried out with nonlinear calibrated parameters for different grades of *Guadua* strip inclination. Models with the inclinations presented in Figure 7 were used.

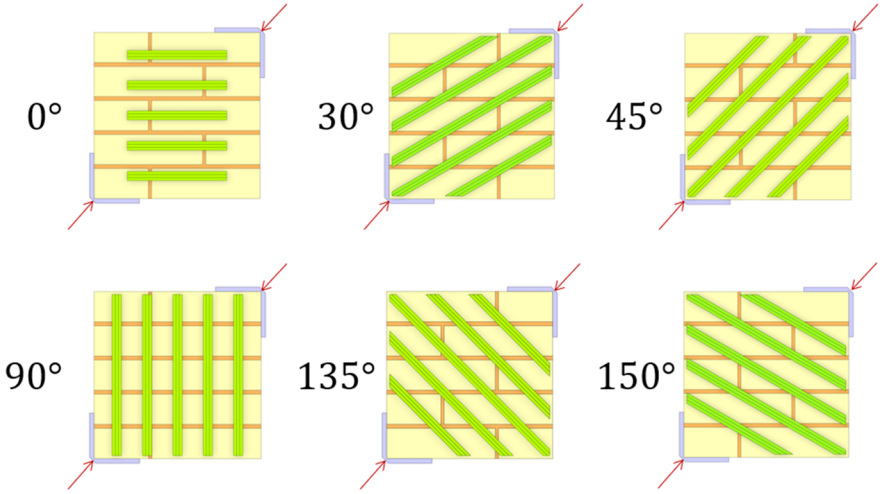

FIGURE 7
Models of reinforced wallettes with different inclinations of Guadua strips under diagonal tension
Source: Authors own creation.

Results

Compression test simulation

The contact between the mortar and the adobe units was modeled as bonded, meaning the surfaces behave as permanently fused with no penetration, separation, or sliding. In contrast, the contact between the steel plates and the wallette was defined as rough, which prevents penetration and sliding by locking the surfaces together upon contact, while still allowing separation.

To analyze the mechanical behavior of the wallette, simulations were conducted using four different mesh sizes. Although all materials were assumed to behave linearly in the initial portion of the response, the coarser meshes produced noticeable variations in stiffness. This is attributed to their reduced ability to capture localized deformations at contact zones, which affects the accuracy of the elastic response. As shown in Figure 8, the selected 15 mm mesh offered a consistent and reliable representation.

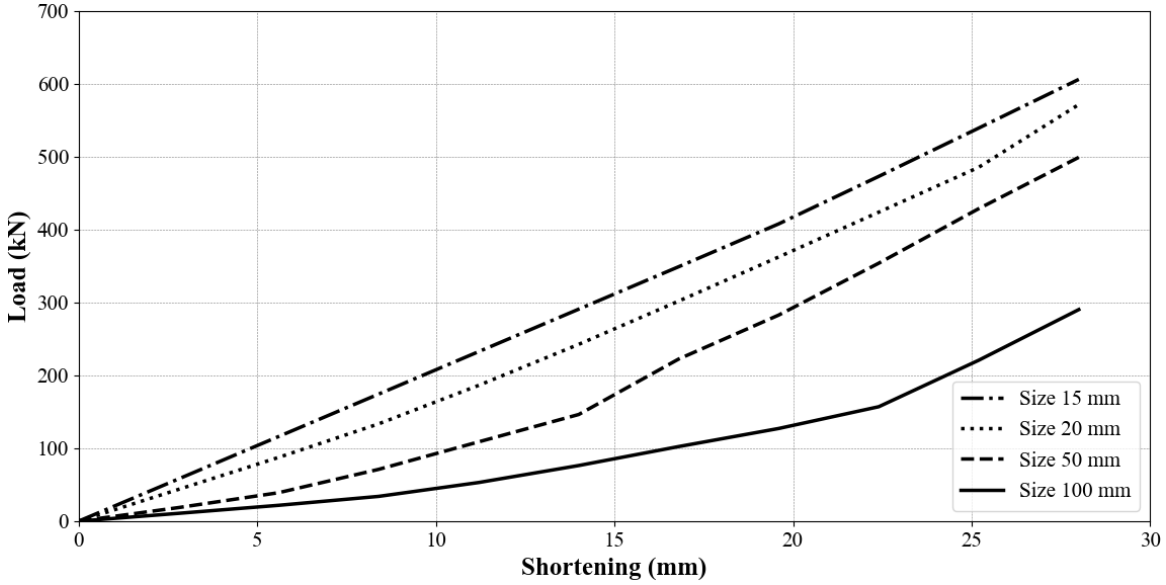

FIGURE 8
Sensitivity analysis of compression wallette without reinforcement
Source: Authors own creation.

Based on these results, a 15 mm mesh size was selected for subsequent simulations. Although a 10 mm mesh was also tested, it yielded only minor differences in the global response compared to the 15 mm mesh, while significantly increasing the computational cost. Therefore, the 15 mm mesh was considered an optimal compromise between accuracy and efficiency. In this configuration, the material properties were defined with a modulus of elasticity of 20 MPa for the adobe units and 8.3 MPa for the mortar in the linear elastic range. For the plastic range, the material response was calibrated using the microplane model, with parameters detailed in Table 2.

TABLE 2
Microplane model parameters in the compression model of the unreinforced wallette

Parameter	Adobe	Mortar
E	20 MPa	8.3 MPa
ν	0.15	0.15
f_c	0.83 MPa	0.55 MPa
f_b	0.91 MPa	0.62 MPa
D	100 MPa²	1 MPa²
σ_{cv}	-32 MPa	-1 MPa
R_c	2	2
γ_t	3.5E-04	5.5E-06
c	3E-05	1E-05
β_t	10 200	11 000
β_c	9 300	9 000

Source: Authors own creation.

By comparing the load-displacement graphs obtained from the numerical model (UWCS, Unreinforced wallette compression simulation) with the averaged experimental data (UWCT, Unreinforced wallette compression test), illustrated in Figure 9, the maximum simulated and experimental stresses were determined.

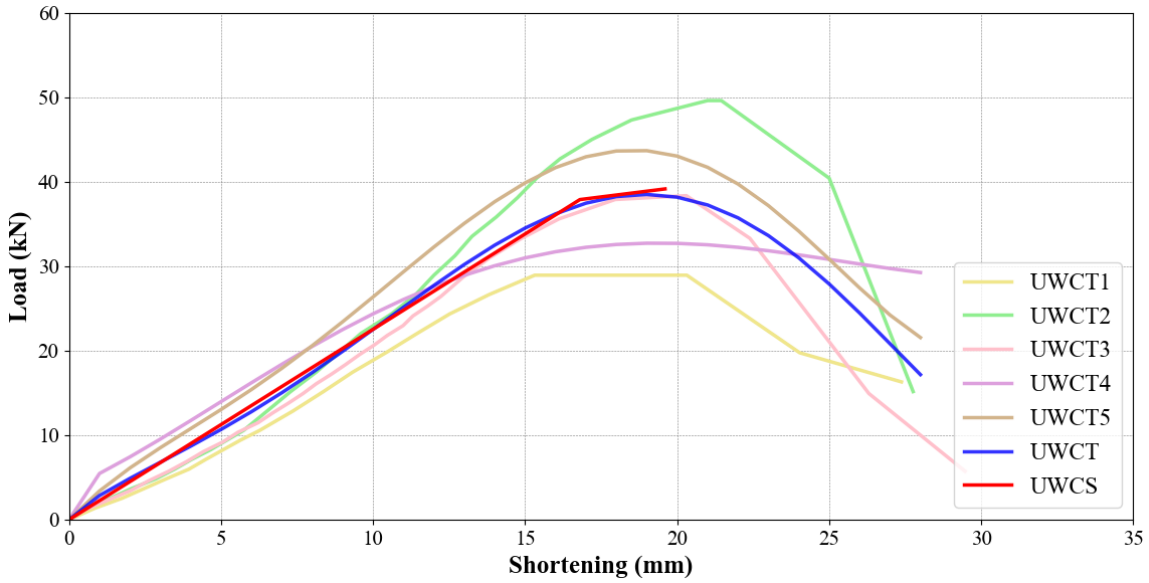

FIGURE 9
Adobe wallette model under compression
Source: Authors own creation.

In Figure 10, the stresses in the corners of the wallette exhibit minimum values of 0.6 MPa. When compared with the experimental results, it is evident that failure typically begins in these locations. This observation is corroborated by the laboratory test results shown in Figure 11, where the failure patterns align with the stress concentrations identified in the simulations.

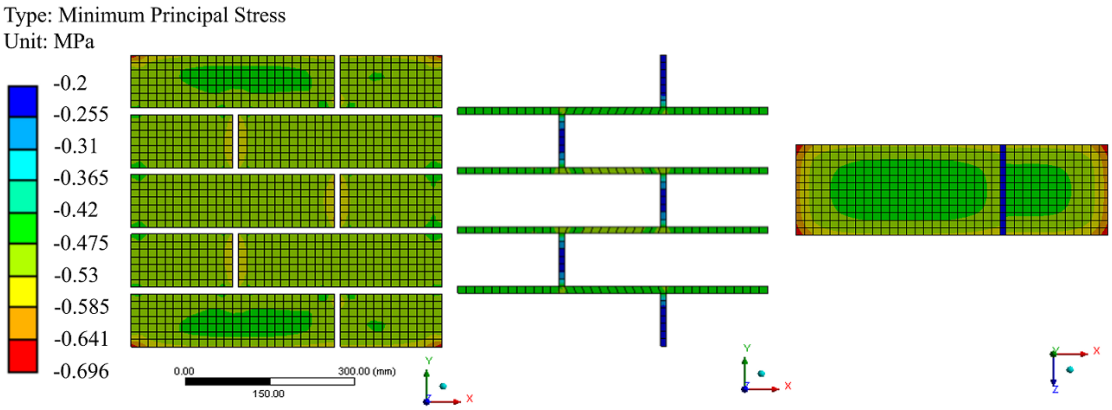

FIGURE 10
Minimum principal stress of the wallette and the mortar under the compression test
Source: Authors own creation.

FIGURE 11
Failure of the masonry wallette under the compression test
Source: Forero, 2022. [21]

With the model calibration, the mechanical behavior of the wallette reinforced with *Guadua* strips was established. Bonded contact type was established both between the *Guadua* strips themselves and between these strips and the wallette's mortar, reflecting the bond developed during the construction process. Similarly, as there was no direct interaction between the adobe units and the *Guadua*, a frictionless contact type was determined.

In the analysis of the linear elastic range, the modulus of elasticity was determined to be 12.5 MPa for the adobe units, 4.5 MPa for the mortar, and 900 MPa for the *Guadua* strips. These values were derived from stress-strain curves obtained from compression tests for the adobe and mortar, and tensile tests for the *Guadua* strips. Poisson's ratio for all materials was consistently set at 0.15, a typical value for such materials, as variations in this parameter have a negligible effect on the simulation results.

After confirming the similarity between the developed model (RWCS, Reinforced wallette compression simulation) and the average behavior of the tested wallettes (RWCT, Reinforced wallette compression test) as illustrated in Figure 12, the model validation was conducted.

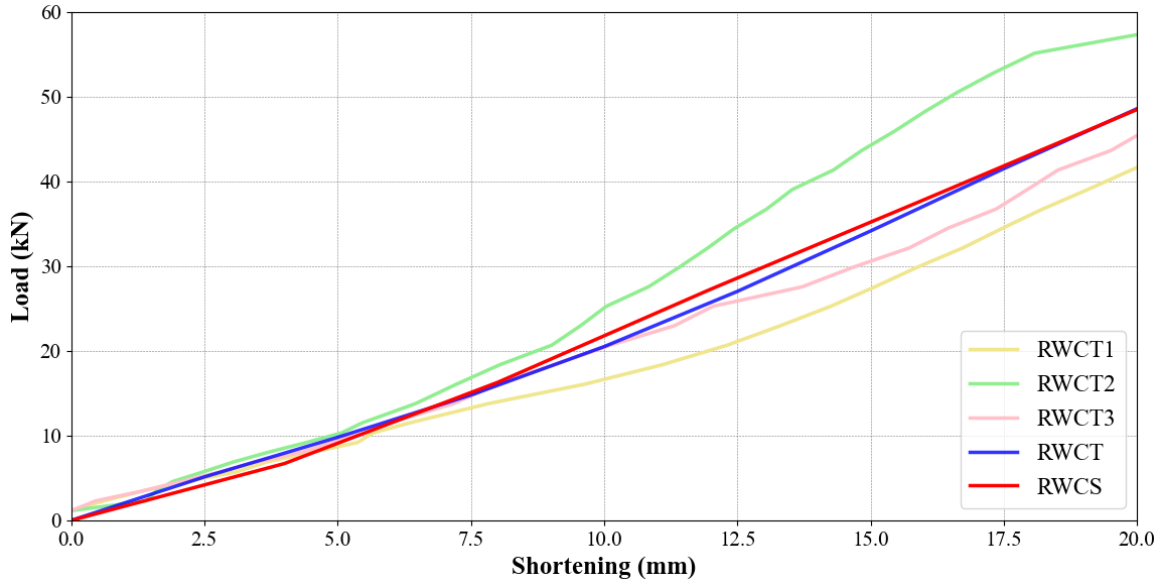

FIGURE 12
Elastic behavior under the compression test of the wallette reinforced vertically with *Guadua* strips
Source: Authors own creation.

Subsequently, various inclinations of *Guadua* strips were proposed for reinforcement. Leveraging the symmetry of the wallette structure, the reinforcement angle was analyzed in 15° increments, ranging from 0° (horizontal configuration) to 90° (vertical configuration), as shown in Figure 4. The analysis revealed that the most effective reinforcement for the wallettes under compression load was achieved at an angle of 90°, as depicted in Figure 13.

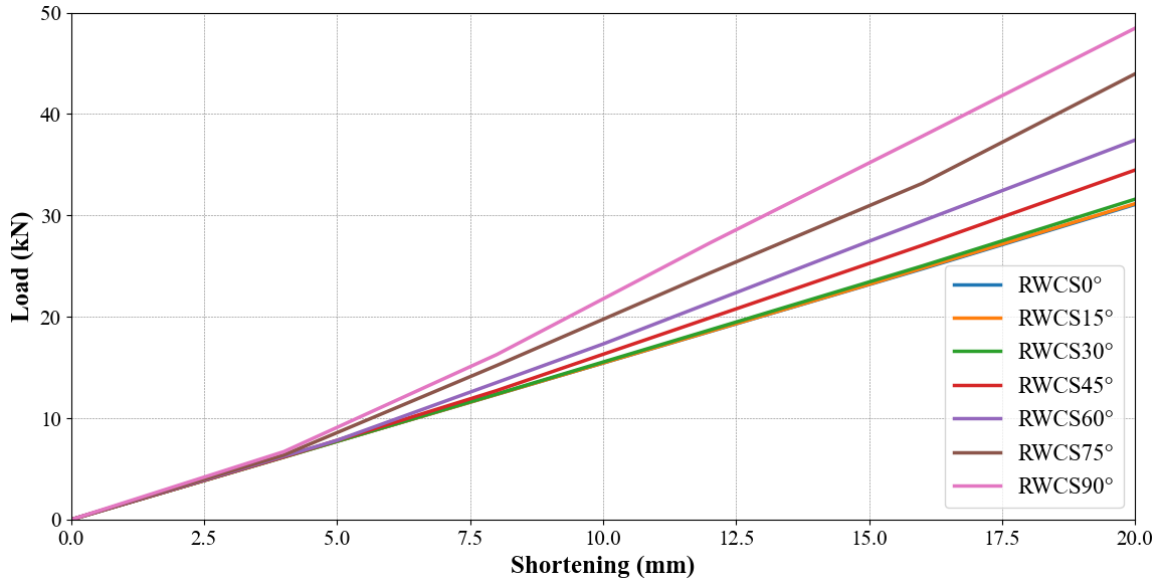

FIGURE 13
Behavior under the compression test of wallettes reinforced with different inclinations of *Guadua* strips
Source: Authors own creation.

In both Figure 12 and Figure 13, an increase in stiffness is observed during the loading process, as indicated by the rising slope of the curves. This behavior may be attributed to the progressive consolidation and

densification of the mortar layers between the adobe blocks, which enhances interfacial contact and improves load transfer as the test progresses.

Diagonal tension test simulation

Following a similar approach to the compression analysis, both linear and non-linear analyses were performed, calibrating the numerical models with experimental test data. To ensure consistency, a 15 mm mesh size was maintained, and the wallette materials were defined within the elastic range: 12 MPa and 7 MPa for Young's modulus of the adobe units and mortar, respectively. For the non-linear range, the following parameters were applied as shown in Table 3.

TABLE 3
Calibrated parameters in the microplane model for the wallette without diagonal tension reinforcement

Parameter	Adobe	Mortar
E	12 MPa	7 MPa
ν	0.15	0.15
f_t	0.04 MPa	0.03 MPa
D	1 MPa²	1 MPa²
σ_{cv}	-1 MPa	-1 MPa
R_c	2	2
γ_t	0.000001	0.0001
γ_c	0.00001	0.0001
β_t	11 000	15 000
β_c	10 000	12 000

Source: Authors own creation.

After calibrating the models, the maximum principal stress in the non-linear range was analyzed, with the results presented in Figure 14. The failure pattern observed in the numerical model closely resembles the experimental results, as shown in Figure 15. The failure in the model occurs at the center of the wallette, particularly at the joints between the adobe blocks and the surrounding areas. This behavior highlights a low resistance in the contact zones between the adobe units, emphasizing their vulnerability under diagonal tension.

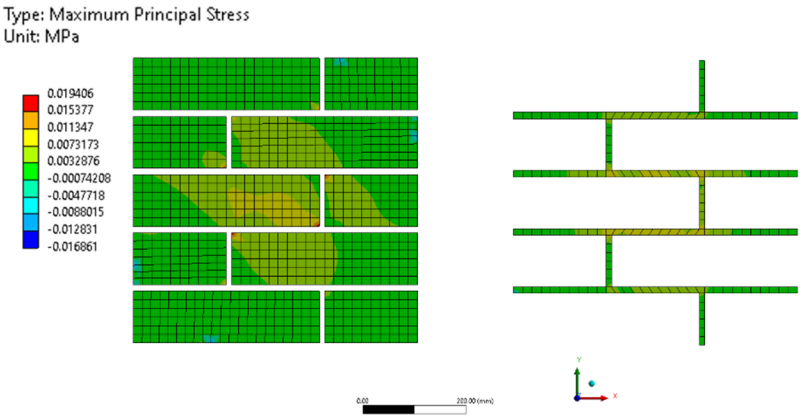

FIGURE 14
Maximum principal stress in the model of unreinforced wallettes under the diagonal tension test
Source: Authors own creation.

FIGURE 15
Failure of masonry wallette under the diagonal tension test
Source: Forero, 2022. [21]

Following the calibration of the unreinforced model, an analysis was conducted on a wallette reinforced with *Guadua* strips. The same parameters were maintained for the wallette, with the Guadua strips modeled using a Young's modulus of 900 MPa. The *Guadua* strips were assumed to behave as orthotropic and elastic materials without non-linear parameters. These assumptions enabled the computational model to simulate the behavior without requiring further calibration, producing representative results, as illustrated in Figure 16.

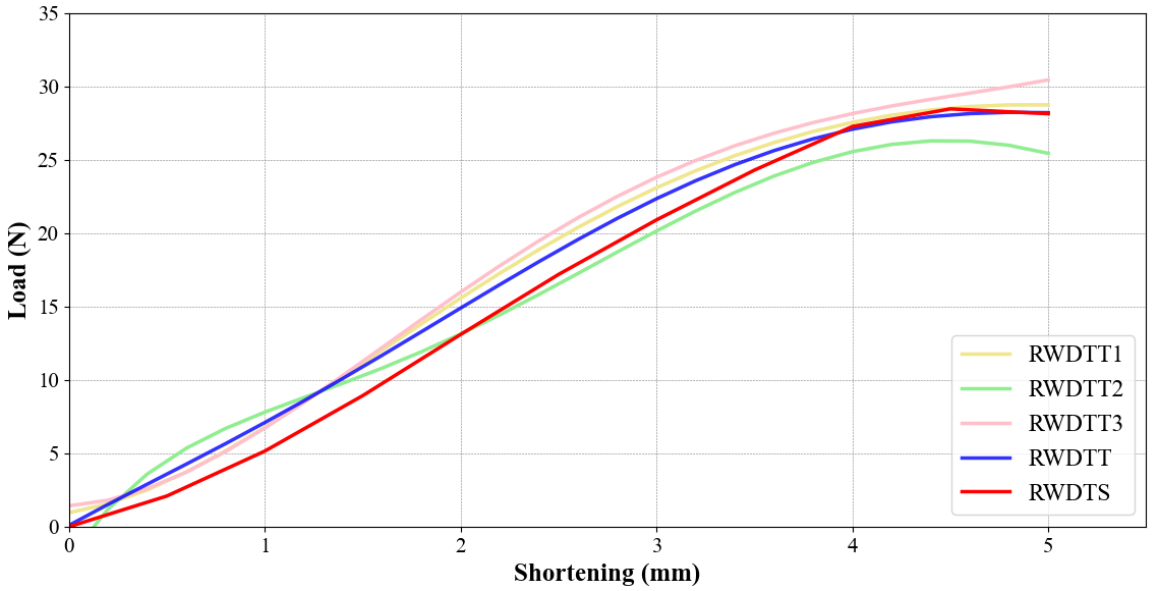

FIGURE 16
Behavior of the wallette model reinforced with Guadua strips inclined at 45° under diagonal tension
Source: Authors own creation.

The numerical simulation of reinforced wallettes produced a representative load-shortening curve (RWDTS, Reinforced Wallette Diagonal Tension Simulation) comparable to the experimental results (RWDTT, Reinforced Wallette Diagonal Tension Test). Figure 17 demonstrates more than a twofold increase in the wallette's capacity under diagonal tension due to *Guadua* strip reinforcement.

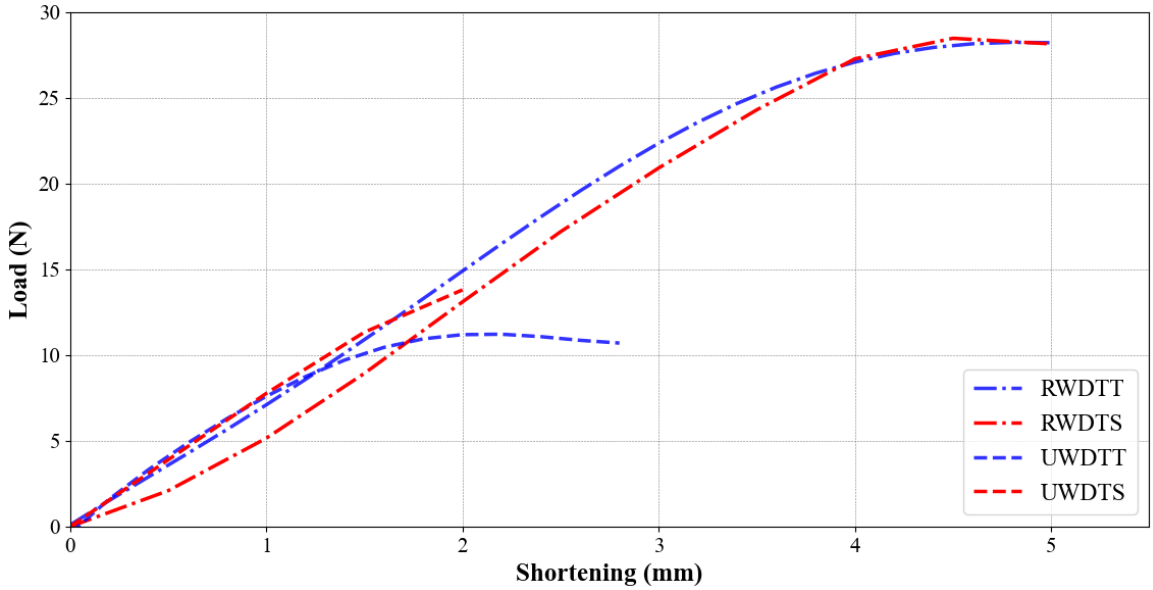

FIGURE 17
Behavior of wallette models with and without reinforcement under diagonal tension test in the non-linear range
Source: Authors own creation.

Using the computational model, a comparison was made for various *Guadua* strip inclinations to evaluate and recommend the optimal reinforcement angle for adobe wallettes. The load-shortening curves for different *Guadua* strip inclinations (RWDTS, Reinforced Wallette Diagonal Tension Simulation) were

analyzed, with the inclinations evaluated every 30°, as illustrated in Figure 7. These simulations considered the load application direction, and the results are presented in Figure 18. It was observed that the behavior of the reinforced wallettes was generally consistent across all inclinations. However, the wallette reinforced with *Guadua* strips at an inclination of 150° exhibited lower maximum resistance and stiffness compared to other configurations. Although this orientation does not align with the principal tensile stress direction in diagonal tension, it was included to highlight the reduced effectiveness of unfavorable reinforcement angles.

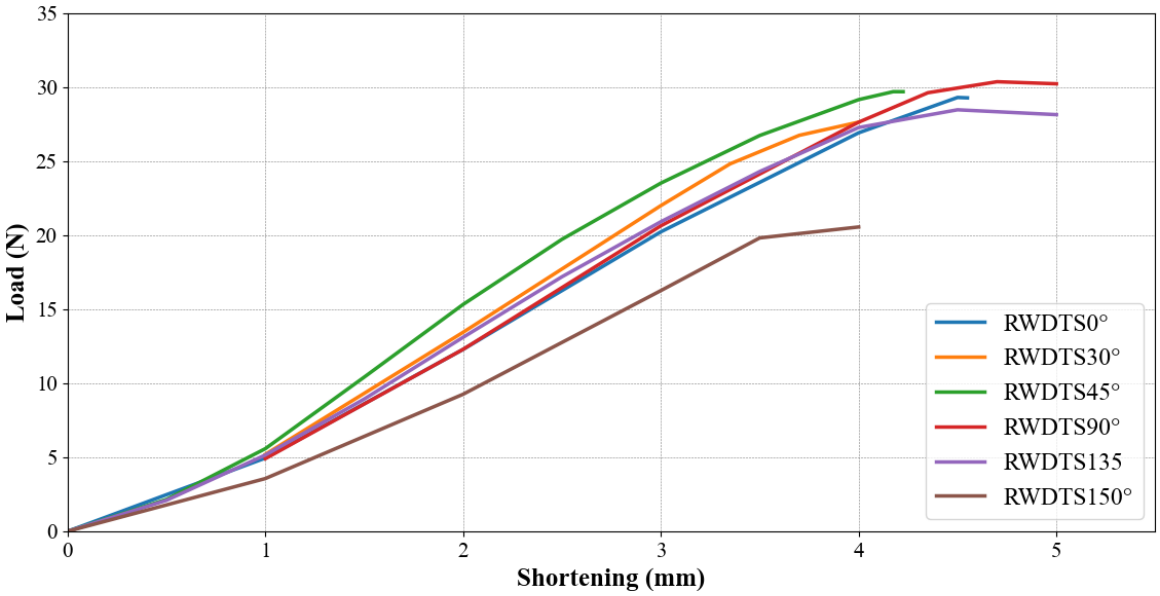

FIGURE 18

Behavior of wallette models with reinforcement in different inclination configurations under the diagonal tension test

Source: Authors own creation.

Conclusions

This study demonstrates that numerical simulation using the finite element method (FEM) is a reliable and effective tool for analyzing the mechanical behavior of adobe wallettes reinforced with *Guadua angustifolia* Kunth strips. The results highlight the significant improvement in the mechanical performance of adobe wallettes under both compression and diagonal tension loads when reinforced with *Guadua* strips.

The analysis of different reinforcement orientations revealed that the configuration at 90° (vertical) consistently offers superior mechanical performance in terms of load-bearing capacity and stiffness. This configuration also presents practical advantages, such as ease of construction, making it the most suitable choice for reinforcing adobe structures in real-world applications. Conversely, the orientation at 150° showed comparatively lower performance, which may limit its practical utility.

In the diagonal tension test simulations, all reinforced wallettes exhibited a marked increase in ultimate resistance compared to their unreinforced counterparts, further validating the effectiveness of *Guadua* strips as a retrofitting material. The reinforcement provided by *Guadua* strips not only enhances the structural stability of adobe wallettes but also addresses critical vulnerabilities, such as low tensile strength, which are common in traditional adobe constructions.

These findings underline the potential of *Guaduaangustifolia* Kunth as a sustainable, cost-effective, and accessible material for retrofitting adobe structures, particularly in regions with limited resources and high seismic vulnerability. Its use aligns with modern engineering practices focused on renewable materials and

sustainable development, offering a practical solution to improve the resilience of adobe constructions against seismic events.

While the numerical model employed is capable of capturing post-peak softening behavior, the curves in this study were truncated at the peak load due to two main limitations: the experimental tests were conducted under load control, preventing observation of the descending branch, and convergence issues in the simulations—especially under diagonal tension—restricted stable computation beyond the peak. This highlights the importance of addressing these challenges to fully characterize the post-peak response of reinforced adobe structures.

Future research could include displacement-controlled experimental setups and improved numerical strategies to overcome the limitations discussed above, as well as large-scale experimental testing to validate the findings of this study. Additionally, exploring applications of *Guadua* reinforcement in heritage infrastructures, where preserving structural integrity and authenticity is critical. Such efforts would contribute to the development of practical guidelines for implementing sustainable retrofitting techniques in diverse contexts.

References

[1] F. Parisi, D. Asprone, L. Fenu, and A. Prota, "Experimental characterization of Italian composite adobe bricks reinforced with straw fibers," Compos Struct, vol. 122, pp. 300–307, Apr. 2015, doi: 10.1016/j.compstruct.2014.11.060.

[2] M. Costi de Castrillo, M. Philokyprou, and I. Ioannou, "Comparison of adobes from pre-history to-date," J Archaeol Sci Rep, vol. 12, pp. 437–448, Apr. 2017, doi: 10.1016/j.jasrep.2017.02.009.

[3] I. Onyegiri and B. U. Iwuagwu, "Traditional Building Materials as a Sustainable Resource and Material for Low Cost Housing in Nigeria: Advantages, Challenges and the Way Forward," International Journal of Research in Chemical, Metallurgical and Civil Engineering, vol. 3, no. 2, Aug. 2016, doi: 10.15242/IJRCMCE.U0716311.

[4] O. A. P. Olukoya and S. Kurt, "Environmental impacts of adobe as a building material: The north cyprus traditional building case," Case Studies in Construction Materials, vol. 4, pp. 32–41, Jun. 2016, doi: 10.1016/j.cscm.2015.12.001.

[5] D. Daudon, Y. Sieffert, O. Albarracín, L. G. Libardi, and G. Navarta, "Adobe Construction Modeling by Discrete Element Method: First Methodological Steps," Procedia Economics and Finance, vol. 18, pp. 247–254, 2014, doi: 10.1016/S2212-5671(14)00937-X.

[6] V. Giamundo, G. Lignola, A. Prota, and G. Manfredi, "Nonlinear Analyses of Adobe Masonry Walls Reinforced with Fiberglass Mesh," Polymers (Basel), vol. 6, no. 2, pp. 464–478, Feb. 2014, doi: 10.3390/polym6020464.

[7] F. Pacheco-Torgal and S. Jalali, "Earth construction: Lessons from the past for future eco-efficient construction," Constr Build Mater, vol. 29, pp. 512–519, Apr. 2012, doi: 10.1016/j.conbuildmat.2011.10.054.

[8] M. Espitia et al., "Mechanical and physical characterization of Guadua angustifolia 'Kunth' fibers from Colombia," Revista UIS Ingenierías, vol. 17, no. 2, pp. 33–40, Mar. 2018, doi: 10.18273/revuin. v17n2-2018003.

[9] D. Silveira, H. Varum, and A. Costa, "Influence of the testing procedures in the mechanical characterization of adobe bricks," Constr Build Mater, vol. 40, pp. 719–728, Mar. 2013, doi: 10.1016/j.conbuildmat.2012.11.058.

[10] M. Giaretton, D. Dizhur, and H. Morris, "Material characterisation of heavy-weight and lightweight adobe brick walls and in-plane strengthening techniques," Constr Build Mater, vol. 310, p. 125309, Dec. 2021, doi: 10.1016/j.conbuildmat.2021.125309.

[11] D. Silveira, H. Varum, A. Costa, and J. Carvalho, "Mechanical Properties and Behavior of Traditional Adobe Wall Panels of the Aveiro District," Journal of Materials in Civil Engineering, vol. 27, no. 9, Sep. 2015, doi: 10.1061/(ASCE)MT.1943-5533.0001194.

[12] A. Caporale, F. Parisi, D. Asprone, R. Luciano, and A. Prota, "Comparative micromechanical assessment of adobe and clay brick masonry assemblages based on experimental data sets," Compos Struct, vol. 120, pp. 208–220, Feb. 2015, doi: 10.1016/j.compstruct.2014.09.046.

[13] G. Araya-Letelier et al., "Experimental evaluation of adobe mixtures reinforced with jute fibers," Constr Build Mater, vol. 276, p. 122127, Mar. 2021, doi: 10.1016/j.conbuildmat.2020.122127.

[14] M. C. M. Parlato, M. Cuomo, and S. M. C. Porto, "Natural fibers reinforcement for earthen building components: Mechanical performances of a low quality sheep wool ('Valle del Belice' sheep)," Constr Build Mater, vol. 326, p. 126855, Apr. 2022, doi: 10.1016/j.conbuildmat.2022.126855.

[15] I. M. G. Bertelsen, L. J. Belmonte, G. Fischer, and L. M. Ottosen, "Influence of synthetic waste fibres on drying shrinkage cracking and mechanical properties of adobe materials," Constr Build Mater, vol. 286, p. 122738, Jun. 2021, doi: 10.1016/j.conbuildmat.2021.122738.

[16] E. Olacia, A. L. Pisello, V. Chiodo, S. Maisano, A. Frazzica, and L. F. Cabeza, "Sustainable adobe bricks with seagrass fibres. Mechanical and thermal properties characterization," Constr Build Mater, vol. 239, p. 117669, Apr. 2020, doi: 10.1016/j.conbuildmat.2019.117669.

[17] L. E. Yamín Lacouture, C. Phillips Bernal, J. C. Reyes Ortiz, and D. Ruiz Valencia, "Estudios de vulnerabilidad sísmica, rehabilitación y refuerzo de casas en adobe y tapia pisada," Apuntes: Revista de estudios sobre patrimonio cultural, vol. 20, no. 2, jul. 2007, [Online]. Available: https://revistas.javeriana.edu.co/index.php/revApuntesArq/article/view/8984

[18] C. J. Whitman, "Heritage Earth Construction and Hygrothermal Comfort: The Challenge of Rebuilding in Central Chile," Key Eng Mater, vol. 600, pp. 186–195, Mar. 2014, doi: 10.4028/www.scientific.net/KEM.600.186.

[19] J. C. Reyes et al., "Seismic retrofitting of existing earthen structures using steel plates," Constr Build Mater, vol. 230, p. 117039, Jan. 2020, doi: 10.1016/j.conbuildmat.2019.117039.

[20] C. Flores Bastidas, C. L. Flores Bastidas, J. I. G. Tsutsumi, and C. P. Takeuchi, "Approach to the Load Resistance in Two Kinds of Bamboo Reinforced Concrete Slab," Adv Mat Res, vol. 261 263, pp. 459–463, May 2011, doi: 10.4028/www.scientific.net/AMR.261-263.459.

[21] J. Forero, "Caracterización mecánica de muretes de adobe reforzados con esterilla de guadua," Universidad Nacional de Colombia, Bogotá, 2022.

[22] N. Quinn, D. D'Ayala, and T. Descamps, "Structural Characterization and Numerical Modelling of Historic Quincha Walls," International Journal of Architectural Heritage, p. 15583058.2015.1113337, Dec. 2015, doi: 10.1080/15583058.2015.1113337.

[23] J. M. Fages, N. Tarque, J. D. Rodríguez-Mariscal, and M. Solís, "Calibration of a total strain crack model for adobe masonry based on compression and diagonal compression tests," Constr Build Mater, vol. 352, Oct. 2022, doi: 10.1016/j.conbuildmat.2022.128965.

[24] I. Zreid and M. Kaliske, "A gradient enhanced plasticity–damage microplane model for concrete," Comput Mech, vol. 62, no. 5, pp. 1239–1257, Nov. 2018, doi: 10.1007/s00466-018-1561-1.

[25] W. B. Krätzig and R. Pölling, "An elasto-plastic damage model for reinforced concrete with minimum number of material parameters," Comput Struct, vol. 82, no. 15–16, pp. 1201–1215, Jun. 2004, doi: 10.1016/j.compstruc.2004.03.002.

[26] F. Gatuingt and G. Pijaudier-Cabot, "Coupled damage and plasticity modelling in transient dynamic analysis of concrete," Int J Numer Anal Methods Geomech, vol. 26, no. 1, pp. 1–24, Jan. 2002, doi: 10.1002/nag.. 188.

[27] J. Lee and G. L. Fenves, "Plastic-Damage Model for Cyclic Loading of Concrete Structures," J Eng Mech, vol. 124, no. 8, pp. 892–900, Aug. 1998, doi: 10.1061/(ASCE)0733-9399(1998)124:8(892).

[28] B. Lei, T. Qi, Y. Li, Z. Jin, and W. Qian, "An enhanced damaged plasticity model for concrete under cyclic and monotonic triaxial compression," European Journal of Mechanics - A/Solids, vol. 100, p. 104999, Jul. 2023, doi: 10.1016/j.euromechsol.2023.104999.

[29] A. Cornejo, S. Jiménez, L. G. Barbu, S. Oller, and E. Oñate, "A unified non-linear energy dissipation-based plastic-damage model for cyclic loading," Comput Methods Appl Mech Eng, vol. 400, p. 115543, Oct. 2022, doi: 10.1016/j.cma.2022.115543.

[30] R. Bakhti, B. Benahmed, A. Laib, and M. T. Alfach, "New approach for computing damage parameters evolution in plastic damage model for concrete," Case Studies in Construction Materials, vol. 16, p. e00834, Jun. 2022, doi: 10.1016/j.cscm.2021.e00834.

[31] S. Oller, E. Oñate, J. Oliver, and J. Lubliner, "Finite element nonlinear analysis of concrete structures using a 'plastic-damage model,'" Eng Fract Mech, vol. 35, no. 1–3, pp. 219–231, Jan. 1990, doi: 10.1016/0013-7944(90)90200-Z.

[32] I. C. Mihai, A. D. Jefferson, and P. Lyons, "A plastic-damage constitutive model for the finite element analysis of fibre reinforced concrete," Eng Fract Mech, vol. 159, pp. 35–62, Jul. 2016, doi: 10.1016/j.engfracmech.2015.12.035.

[33] T. Yu, J. G. Teng, Y. L. Wong, and S. L. Dong, "Finite element modeling of confined concrete-II: Plastic-damage model," Eng Struct, vol. 32, no. 3, pp. 680–691, Mar. 2010, doi: 10.1016/j.engstruct.2009.11.013.

[34] Z. P. Bažant and P. G. Gambarova, "Crack Shear in Concrete: Crack Band Microplane Model," Journal of Structural Engineering, vol. 110, no. 9, pp. 2015–2035, Sep. 1984, doi: 10.1061/(ASCE)0733-9445(1984)110:9(2015).

Notes

* Research article

How to cite this article: J D Perilla Novoa, J E Muñoz Rodrguez, M Molina Herrera, C P Takeuchi Tam, "Numerical Simulation of Adobe Wallettes under Compression and Diagonal Tension with and without Reinforcement of Spaced *Guadua angustifolia* Kunth Strips" Ing. Univ. vol. 29, 2025. https://doi.org/10.11144/Javeriana.iued29.nsaw